Published in: Coloma Ribera *et al.* Appl. Phys. Lett. **105**, 131601 (2014)
http://dx.doi.org/10.1063/1.4896993

Surface and sub-surface thermal oxidation of thin ruthenium films

R. Coloma Ribera,[1,a)] R.W.E. van de Kruijs,[1] S. Kokke,[2] E. Zoethout,[2] A. E. Yakshin,[1] and F. Bijkerk[1]

[1]MESA$^+$ Institute for Nanotechnology, University of Twente, P.O. Box 217, 7500 AE Enschede, The Netherlands.
[2]FOM Dutch Institute for Fundamental Energy Research (DIFFER), P.O. Box 1207, 3430 BE Nieuwegein, The Netherlands.

Abstract

A mixed 2D (film) and 3D (nano-column) growth of ruthenium oxide has been experimentally observed for thermally oxidized polycrystalline ruthenium thin films. Furthermore *in situ* x-ray reflectivity upon annealing allowed the detection of 2D film growth as two separate layers consisting of low density and high density oxides. Nano-columns grow at the surface of the low density oxide layer, with the growth rate being limited by diffusion of ruthenium through the formed oxide film. Simultaneously with the growth of the columns, sub-surface high density oxide continues to grow limited by diffusion of oxygen or ruthenium through the oxide film.

Keywords: surface oxidation, ruthenium, ruthenium oxide, x-ray reflectivity, thin films

Ruthenium thin films and its oxidized compounds raised great interest in many applications in the recent years.[1] Ru has turned out to be the most active catalyst in the synthesis of ammonia,[2,3] while RuO_2 has shown to be an excellent oxidation catalyst in heterogeneous catalysis[4] and electrocatalysis.[5] Other applications for Ru thin films are as bottom electrode in VLSI capacitors based on high dielectric materials,[6] or as capping layer for optics designed for extreme ultraviolet lithography (EUVL)[7,8,9] due to its low-oxidation properties.[10] Oxidation of monocrystalline Ru was extensively investigated during the last decades.[11,12,13,14,15,16,17,18] Recently, oxide thin films and 3D clusters were observed during thermal oxidation of single crystalline Ru.[19,20] For polycrystalline Ru no 3D clusters have been seen, with only thin film oxide growth being observed.[21,22,23]

In this letter we report on the simultaneous 2D (thin film) and 3D (nano-column) growth of ruthenium oxide experimentally observed for thermally oxidized polycrystalline Ru thin films. Furthermore it is also found that the thin film oxide does not grow as a single layer but a combination of two layers on top of each other.

To determine parameters of nanometer range thin films and dynamics of their growth accurately, an *in situ* technique needs to be applied. Previously *in situ* spectroscopic ellipsometry (SE) was used to study growth of thin RuO_2 films during thermal oxidation of Ru.[24,25] However it should be noted that extracting information from SE involves reconstruction of both optical constants and layered structure, a process which is often

[a)] Author to whom correspondence should be addressed. Electronic mail: r.colomaribera@utwente.nl. Tel.: +31 53 489 4431.

uniquely determined. We used *in situ* hard x-ray reflectivity measurements for monitoring thermal oxidation of Ru thin films. The changes of the in-depth electron density distribution were accurately determined from the changes of the reflectivity patterns during the thin film growth. This provided us with information about densities, thicknesses and intermixing/roughnesses of the formed RuO_x and remaining Ru layers during the oxidation process. Combining this with Auger electron spectroscopy, angular-resolved x-ray photoelectron spectroscopy, atomic force microscopy, x-ray diffraction and high-resolution transmission electron microscopy, we present a detailed description of surface and sub-surface oxidation of the ruthenium thin films and propose a model for concurrent 2D and 3D ruthenium oxide growth.

Ten nanometer thick Ru films were deposited onto natively oxidized super-polished Si substrates using DC magnetron sputtering (1×10^{-4} mbar Ar) in a Ultra High Vacuum (UHV) setup with base pressure $<1 \times 10^{-8}$ mbar. Since Ru and Si intermix upon annealing,[26,27] an additional 15 nm SiO_2 diffusion barrier was deposited on top of the Si substrate before Ru deposition. SiO_2 was chosen for this purpose due to its low enthalpy of formation of -910.7 $kJ \cdot mol^{-1}$,[28] compared to -32.4 and -26.0 $kJ \cdot mol^{-1}$ for RuSi and Ru_2Si_3, respectively.[29] Layer thicknesses were monitored with quartz mass balances during deposition and used as initial fit parameters for x-ray reflectivity analysis.

The deposited Ru films were thermally oxidized at temperatures between 150 to 500°C for different amount of time. X-ray reflectivity (XRR) measurements were conducted *in situ* during annealing using a PANalytical Empyrean X-Ray diffractometer (Cu-Kα radiation, 0.154 nm), equipped with an Anton Paar thermal stage.[30] Before annealing, the alignment of the sample position with respect to the impinging x-ray beam was performed and a reference XRR reflectivity curve was recorded. After heating the sample to an elevated temperature, the sample position with respect to the beam was realigned to correct for thermal expansion and possible misalignment, and subsequent XRR scans were recorded during annealing.

X-ray reflectivity curves were analyzed using the GenX software.[31] A layered model of the structure was composed that consists of the Si substrate, a SiO_2 layer, a Ru layer and an oxide layer. Hard x-rays used will fully penetrate the films. However the reflectivity is dominated by the interfaces with high optical contrast such as vacuum/RuO_x, RuO_x/Ru, and Ru/SiO_2. The SiO_2/Si interface has very low optical contrast and does not affect the analysis. The GenX program varied thickness, roughness and density of each of the layers in order to minimize the differences between model simulations and experimental data. Layer thicknesses and layer densities were determined with accuracies of ±0.1 nm and ±0.3 $g \cdot cm^{-3}$, respectively. As an example, measured and simulated XRR data for both an as deposited Ru film, and a sample annealed at 400°C for 20 minutes are presented in Figs. 1(a) and (b), respectively.

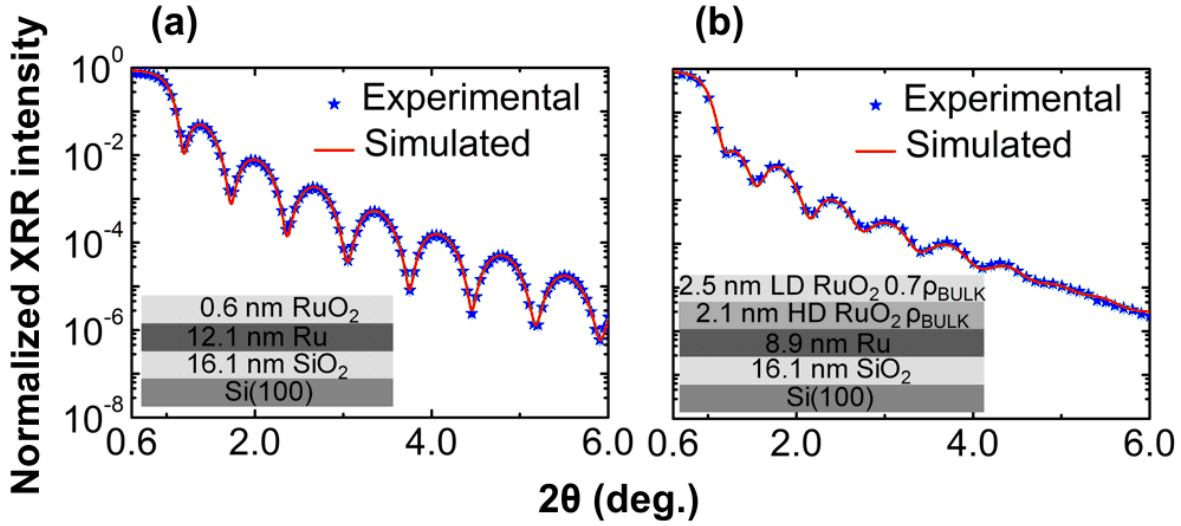

FIG. 1. (Color online) Experimental (stars) and simulated (line) specular x-ray reflectivity (XRR) data for (a) an as deposited sample and (b) a sample annealed at 400°C for 20 minutes. Left-bottom (a,b) inset shows the layered model used for each simulation.

According to XRR of the as-deposited sample (see Fig. 1(a)), there exists a RuO_2 layer of 0.6±0.1 nm on top of Ru. The presence of a monolayer (ML) of oxide on the as-deposited sample was confirmed by XPS measurements. As a low-oxidation material,[10] Ru is known to remain metallic, and only 1ML of oxide is typically chemisorbed at room temperature.[4,32,33,34,35] With increasing temperature, the Ru layer oxidizes further and XRR suggests a gradual growth of a low density oxide layer of approximately 6.0±0.3 $g \cdot cm^{-3}$. Above 325°C, XRR data cannot be modeled using a single low density oxide layer and there is a need for a 2-layer oxide model to describe the thin film oxide growth (see Fig. 1(b)). In this model, a low density (LD) RuO_2 layer is formed on top of a high density (HD) RuO_2 layer, with LD and HD oxide densities being 5.3±0.3 and 6.8±0.3 $g \cdot cm^{-3}$, respectively, which corresponds to 70% and 100% of the bulk RuO_2 density. Angular-resolved photoelectron spectroscopy (AR-XPS) confirms a gradation of the oxide film and indicates that the top part of the layer is oxygen rich, suggesting a RuO_x/RuO_2 ($2<x\leq3$) layer structure.

Fig. 2 (left-axis) shows an example of the oxide layer thickness (low density and high density) and Ru consumption as derived from XRR, as function of annealing time at 400°C. The low density RuO_2 layer (triangles) rapidly saturates at a thickness of approximately 3 nm, while the high density RuO_2 layer (circles) continues to grow. The Ru layer thickness (squares) decreases over time, consistent with the consumption of Ru during formation of RuO_2, and is plotted as Ru loss in Fig. 2. The ratio of thicknesses between the total RuO_2 formed (low density and high density) and Ru lost in time is plotted in Fig. 2 (right-axis, stars) and shows a constant value of ~1.2. Distinctly, based on calculations assuming bulk densities this ratio is expected to be 2.3. This surprising discrepancy has been resolved when studying morphology of the sample surface with AFM, XRD and HR-TEM.

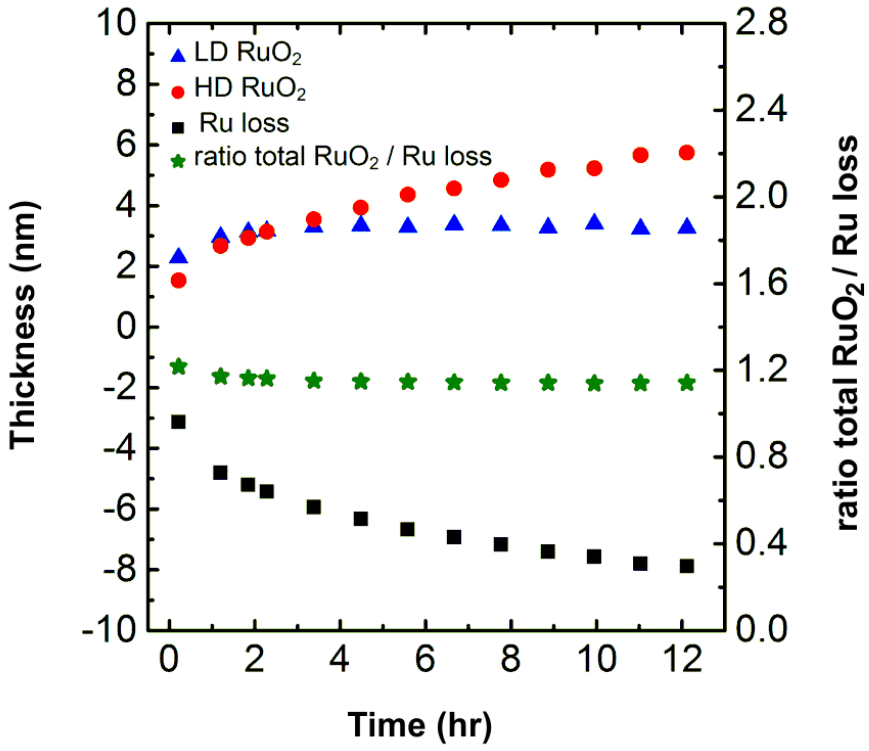

FIG. 2. (Color online) Left-axis: RuO_2 thickness and Ru loss as a function of annealing time for 400°C. Low density (LD) RuO_2 thickness (triangles), high density (HD) RuO_2 thickness (circles) and Ru loss (squares) are plotted. Right-axis: ratio between total RuO_2 formed (summed low density and high density) and Ru loss as a function of annealing time for 400°C (stars). The layer thicknesses were determined with the accuracy of ±0.1 nm.

The top surface of the oxidized Ru surface was studied by atomic force microscopy (AFM) for the samples annealed for 20 minutes at temperatures between 150 and 500°C. Fig. 3 shows the 1x1μm AFM images for as deposited Ru (a), and 20 minutes annealed samples at 175°C (b), 200°C (c) and 300°C (d). The as deposited and 175°C annealed samples present a similar root mean square (RMS) value of ~0.25 nm (see Figs. 3(a) and 3(b)). The surface morphology start to change significantly when the samples are annealed at 200°C. 3D columns appear at the surface and grow in size with increasing oxidation temperature (Figs. 3(c) and 3(d)). Line profiles along the lines indicated in Figs. 3(c) and 3(d) are presented in Figs. 3(e) and 3(f) and show the evolution of the columns from an average height of 7 nm at 200°C to an average height of 30 nm at 300°C. High spatial resolution Auger electron spectroscopy (AES) analysis has confirmed the presence of ruthenium oxide in both columns and in the areas between columns on the surface.

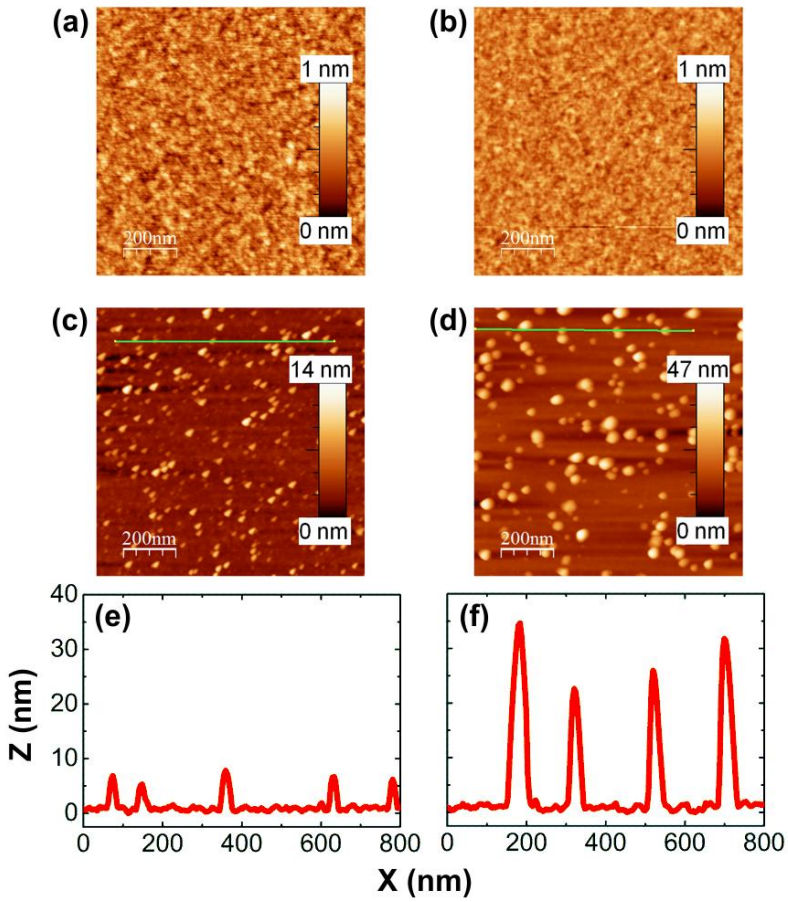

FIG. 3. (Color online) Atomic force microscopy (AFM) images (1x1μm) of the as deposited (a), and 20 minutes annealed samples at 175°C (b), 200°C (c), and 300°C (d). Line profiles of the 20 minutes annealed samples at 200°C (e), and 300°C (f), are represented by the straight lines shown in the AFM images (c) and (d), respectively.

X-ray diffraction patterns were recorded for all annealed samples. The magnetron sputtered Ru layer exhibited a hcp polycrystalline structure[1,36,37] over the entire temperature range, with intensities reducing at higher temperatures due to Ru consumption during RuO_2 growth. For Ru, no angular dependence of the diffracted intensity was observed apart from that induced by the illumination geometry, and as such a random orientation of crystallites is suggested. RuO_2 peaks typical for rutile-like crystalline structure[1] were detected that showed two types of diffraction patterns. One pattern was detected above 275°C and belonged to larger oriented crystallites, with (101) planes being nearly perpendicular to the sample surface normal. Another pattern was detected above 375°C and belonged to smaller crystallites showing random orientations. It appeared that the larger crystallites actually matched very well the average height of the surface 3D columns determined by AFM. The smaller crystallites matched the thickness of the 2D oxide film when measured close to the growth direction of the film. Note that the vertical sizes of the columns were more than ten times larger than the thickness of the thin oxide film (see for example the sample annealed at 300°C, Fig. 3(f) and Fig. 4 (first circle)).

Below we calculated the ratio of the consumed Ru to the formed Ru oxide taking into account both oxides, in the thin film and in the columns. From the AFM images, an effective volume for the RuO_2 columns can be extracted after a geometric convolution correction. This RuO_2 volume, divided by the AFM scan area, yields an "effective thickness", the value as if all the amount of RuO_2 observed in the 3D columns would be distributed in a flat continuous layer. This is depicted in Fig. 4 (closed squares) together with the thin Ru oxide film thickness (solid circles). The similar growth of these two curves indicates that both oxides, the thin film and the columns, have similar volume growth rate, which is important for further discussion. Fig. 4 also shows reduction of the Ru layer thickness (open triangles) with annealing. When the RuO_2 "effective thickness" determined from AFM is added to the RuO_2 thickness obtained from XRR and then divided by the Ru loss, a ratio of 3.5 is achieved at low temperatures (Fig. 4, dashed line), consistent with the larger contribution of the low density Ru oxide layer growth at low temperatures. For the high temperatures, the ratio approaches the calculated value of 2.3, consistent with the predominant high density RuO_2 growth observed from XRR.

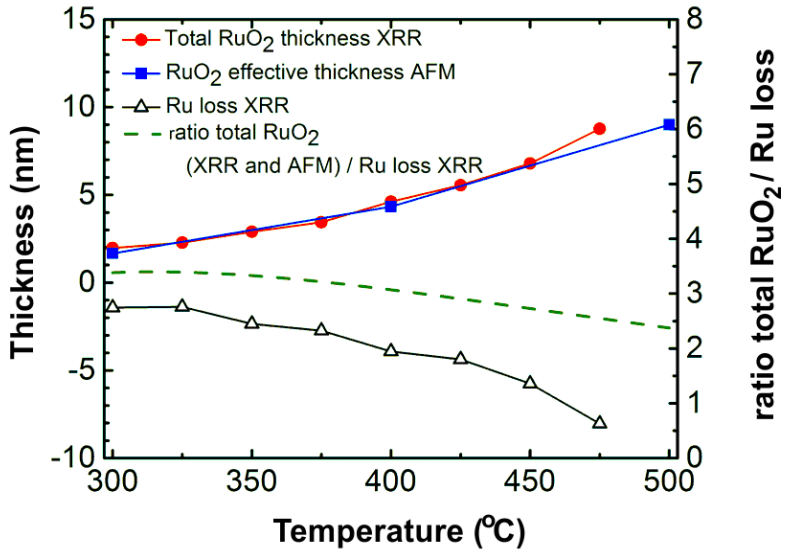

FIG. 4. (Color online) Oxide thickness and Ru loss as a function of annealing temperature for 20 min annealed samples in the range of 300-500°C. Total RuO_2 thickness (summed low density and high density) obtained from XRR is presented by closed circles. The RuO_2 "effective thickness" from AFM analysis is depicted by closed squares. The Ru loss from XRR is shown by open triangles. The ratio between total RuO_2 (summed XRR and AFM amount) and Ru loss from XRR is represented by the dashed line. The accuracies of the layer thicknesses determined by XRR and AFM analysis are ±0.1 and ±0.3 nm, respectively.

High resolution transmission electron microscopy (HR-TEM) showed more details on the formed structure, as depicted by the cross-section of a 20 minutes annealed Ru sample at 300°C (Fig. 5). First of all it confirms the polycrystallinity of the Ru layer with different crystal orientations. Ruthenium thin film oxide on top of polycrystalline Ru is visible (Fig. 5(a)). Its thickness is in a very good agreement with the one obtained from XRR. Some crystalline parts in this ruthenium oxide layer are observed. But it is too thin to conclude if the crystalline part belongs to the ruthenium oxide layer itself or to the Ru layer which overwhelms the very thin top layer in the HR-TEM image. The majority of the surface

columns were detached from the surface during TEM preparation. However, it is well visible that the columns have rectangular- rather than spherical-like shape as imaged by AFM. They have an aspect ratio of about 1:3 on average (for the sample at 300°C) demonstrating strongly anisotropic growth. The columns grow monocrystalline. HR-TEM at Fig. 5(b) resolves the (101) planes that are positioned at 115° with respect to the longer side of the column. This side corresponds to (110) crystal plane taking into account the rutile-like structure of the oxide. For this structure (110) surface has the lowest energy,[38] which explains why it is the most abundant surface of the observed columns.

It cannot be observed by TEM if the columns grow at the surface of Ru or at the surface of the ruthenium oxide thin layer. The columns could in principle grow as continuation of the Ru grains with the proper orientation. In that case Ru would act as a seeding layer for the columns. However the columns are typically a factor of ten larger in height compared to the oxide film thickness. If they would originate at the initial Ru surface, they would have already been detected by AFM for the sample annealed at 175°C (Fig. 3(b)). According to XRR at this temperature there is already a 0.85 nm low density thin film oxide formed at the surface, which is expected to be a closed layer. So it is still most likely that the columns grow at the surface of the formed thin ruthenium oxide layer rather than the surface of Ru layer. Note that the volume growth rate of the columns is similar to the one of the thin oxide film as mentioned above. Obviously both rates are limited by diffusion of atoms through the thin oxide film, ruthenium upwards and oxygen downwards.

The remaining question is why the nano-columns prefer to grow in 3D mode at the surface of the ruthenium oxide layer and not to continue growing in the initial 2D thin film mode. We suggest that there are several factors contributing to the coexistence of the 2D and 3D growth. Oxidation of ruthenium film starts with the formation of a low density RuO_x ($2<x\leq3$) layer. In the process of further oxidation this low density oxide layer is always present on top but is limited to a maximum of 3 nm. The reduced supply of ruthenium atoms that have to diffuse through the ruthenium oxide layer towards the surface and the unlimited supply of oxygen at the surface are the possible reasons why the oxygen rich low density oxide layer is initially formed at the surface. Below this layer a higher density stoichiometric RuO_2 will grow during further oxidation. Up to a certain thickness the oxide film remains quasi-amorphous to keep the minimum energy interface with ruthenium. At about 200°C, because of the rather high mobility of Ru or Ru-O precursors at the surface,[20] the first crystalline RuO_2 nuclei will form at the very surface, with Ru being supplied from the bottom via diffusion through the oxide film. And since the RuO_x top layer with a rather disordered structure does not support growth of a crystalline structure along the surface, RuO_2 crystallites will continue growing in the vertical direction. We detect the first crystalline columns at 275°C when the oxide film still stays quasi-amorphous. At 375°C this film starts to crystallize turning polycrystalline. At that moment the columns already become stable and continue growing at the expense of all the ruthenium reaching the surface.

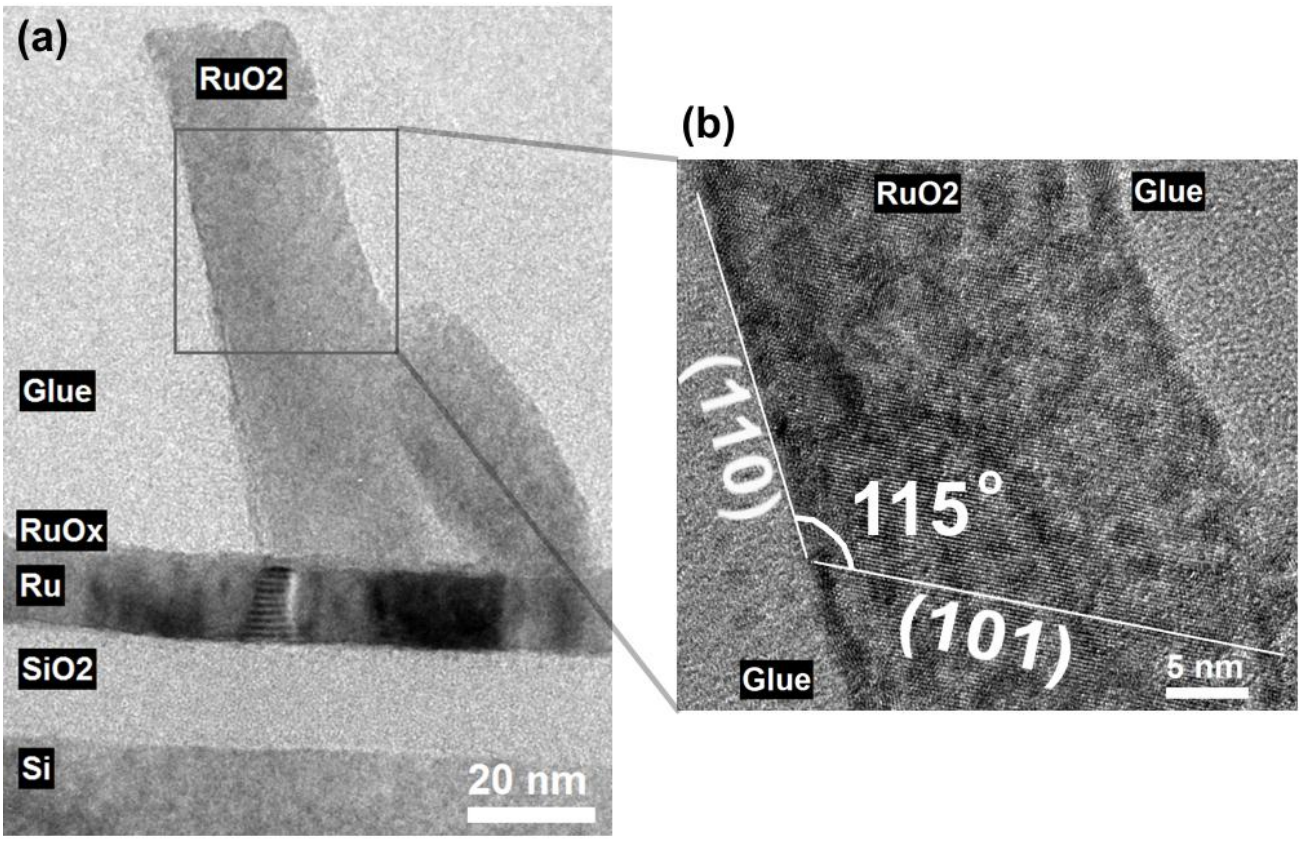

FIG. 5. (Color online) Cross-sectional HR-TEM images of the 20 minutes annealed sample at 300°C. Rectangular-like tilted nano-columns attached to the film surface, showing the strongly anisotropic growth (a). Zoom view of the monocrystalline RuO_2 column with the resolved (101) planes that go from side to side of the column (b). Note that the growth direction of the column is parallel to the (110) RuO_2 planes, forming an angle of 115° with the (101) planes.

In summary, a mixed 2D and 3D growth of Ru oxide has been experimentally observed for thermally oxidized polycrystalline Ru thin films. Below a threshold temperature of 200°C there is approximately one monolayer of thin film low density RuO_x ($2<x\leq3$) on the Ru surface formed. Above 200°C, RuO_2 nano-columns are detected on the surface, growing in size with temperature and annealing duration. Simultaneously with the growth of the columns, sub-surface oxidation continues. The low density oxide film is followed by the formation of a near bulk density RuO_2 thin layer. The total amount of oxide formed, including 2D films and 3D nano-columns, is consistent with the reduction of the Ru layer thickness.

Acknowledgements

This work is part of the research programme 'Controlling photon and plasma induced processes at EUV optical surfaces (CP3E)' of the 'Stichting voor Fundamenteel Onderzoek der Materie (FOM)', which is financially supported by the 'Nederlandse Organisatie voor Wetenschappelijk Onderzoek (NWO)'. The CP3E programme is co-financed by Carl Zeiss SMT and ASML. We also acknowledge financial support from Agentschap NL (EXEPT project).

References

[1] H. Over, Chemical Reviews **112** (6), 3356 (2012).
[2] O. Hinrichsen, F. Rosowski, M. Muhler, and G. Ertl, Chemical Engineering Science **51** (10), 1683 (1996).
[3] K. Honkala, A. Hellman, I. N. Remediakis, A. Logadottir, A. Carlsson, S. Dahl, C. H. Christensen, and J. K. Norskov, Science **307** (5709), 555 (2005).
[4] H. Over, Y. D. Kim, A. P. Seitsonen, S. Wendt, E. Lundgren, M. Schmid, P. Varga, A. Morgante, and G. Ertl, Science **287** (5457), 1474 (2000).
[5] S. Trasatti, Electrochimica Acta **45** (15–16), 2377 (2000).
[6] A. Grill, W. Kane, J. Viggiano, M. Brady, and R. Laibowitz, Journal of Materials Research **7** (12), 3260 (1992).
[7] S. Bajt, H. N. Chapman, N. Nguyen, J. Alameda, J. C. Robinson, M. Malinowski, E. Gullikson, A. Aquila, C. Tarrio, and S. Grantham, Appl. Opt. **42** (28), 5750 (2003).
[8] S. Bajt, Z. R. Dai, E. J. Nelson, M. A. Wall, J. B. Alameda, N. Q. Nguyen, S. L. Baker, J. C. Robinson, J. S. Taylor, A. Aquila, and N. V. Edwards, Journal of Micro/Nanolithography, MEMS, and MOEMS **5** (2), 023004 (2006).
[9] E. Louis, A. E. Yakshin, T. Tsarfati, and F. Bijkerk, Progress in Surface Science **86** (11-12), 255 (2011).
[10] H. J. T. Ellingham, Journal of the Society of Chemical Industry **63** (5), 125 (1944).
[11] T. E. Madey, H. Albert Engelhardt, and D. Menzel, Surface Science **48** (2), 304 (1975).
[12] C. Corriol, F. Calleja, A. Arnau, J. J. Hinarejos, A. L. Vázquez de Parga, W. A. Hofer, and R. Miranda, Chemical Physics Letters **405** (1–3), 131 (2005).
[13] Y. D. Kim, S. Wendt, S. Schwegmann, H. Over, and G. Ertl, Surface Science **418** (1), 267 (1998).
[14] C. Stampfl, S. Schwegmann, H. Over, M. Scheffler, and G. Ertl, Physical Review Letters **77** (16), 3371 (1996).
[15] H. Over, Progress in Surface Science **58** (4), 249 (1998).
[16] Y. B. He, M. Knapp, E. Lundgren, and H. Over, The journal of physical chemistry. B **109** (46), 21825 (2005).
[17] S. Poulston, M. Tikhov, and R. M. Lambert, Langmuir **13** (20), 5356 (1997).
[18] M. Knapp, A. P. Seitsonen, Y. D. Kim, and H. Over, The Journal of Physical Chemistry B **108** (38), 14392 (2004).
[19] B. Herd, M. Knapp, and H. Over, The Journal of Physical Chemistry C **116** (46), 24649 (2012).
[20] B. Herd and H. Over, Surface Science **622** (0), 24 (2014).
[21] Y. B. He, A. Goriachko, C. Korte, A. Farkas, G. Mellau, P. Dudin, L. Gregoratti, A. Barinov, M. Kiskinova, A. Stierle, N. Kasper, S. Bajt, and H. Over, The Journal of Physical Chemistry C **111** (29), 10988 (2007).
[22] Z. Li, T. Schram, L. Pantisano, T. Conard, S. Van Elshocht, W. Deweerd, S. De Gendt, K. De Meyer, A. Stesmans, S. Shamuilia, V. V. Afanas'ev, A. Akheyar, D. P. Brunco, N. Yamada, and P. Lehnen, Journal of Applied Physics **101** (3), 034503 (2007).
[23] E. V. Jelenkovic and K. Y. Tong, Journal of Vacuum Science & Technology B: Microelectronics and Nanometer Structures **22** (5), 2319 (2004).
[24] P. Hones, F. Lévy, T. Gerfin, and M. Grätzel, Chemical Vapor Deposition **6** (4), 193 (2000).
[25] P. Hones, T. Gerfin, and M. Gratzel, Applied Physics Letters **67** (21), 3078 (1995).
[26] L. Perring, F. Bussy, J. C. Gachon, and P. Feschotte, Journal of Alloys and Compounds **284** (1–2), 198 (1999).
[27] L. Pasquali, N. Mahne, M. Montecchi, V. Mattarello, and S. Nannarone, Journal of Applied Physics **105** (4), 044304 (2009).
[28] D.R. Lide, *CRC Handbook of Chemistry and Physics: A Ready-reference Book of Chemical and Physical Data*. (CRC Press, 2004).
[29] G. Borzone, R. Raggio, and R. Ferro, J Min Met **38**, 249 (2002).

[30] R. Resel, E. Tamas, B. Sonderegger, P. Hofbauer, and J. Keckes, Journal of Applied Crystallography **36** (1), 80 (2003).
[31] M. Bjorck and G. Andersson, Journal of Applied Crystallography **40** (6), 1174 (2007).
[32] A. Bottcher and H. Niehus, The Journal of Chemical Physics **110** (6), 3186 (1999).
[33] R. Blume, H. Niehus, H. Conrad, A. Böttcher, L. Aballe, L. Gregoratti, A. Barinov, and M. Kiskinova, The Journal of Physical Chemistry B **109** (29), 14052 (2005).
[34] One monolayer (1 ML) corresponds to a coverage of as many absorbates on the surface as metal atoms in the topmost layer.
[35] Y. S. Huang, H. L. Park, and F. H. Pollak, Materials Research Bulletin **17** (10), 1305 (1982).
[36] A. S. Alagoz, J.D. Kamminga, S. Y. Grachev, T.M. Lu, and T. Karabacak, in *2009 MRS Fall Meeting & Exhibit*, edited by E. Lilleodden J. Lou, B. Boyce, L. Lu, P.M. Derlet, D. Weygand, J. Li, M.D. Uchic, E. Le Bourhis (MRS Online Proceedings Library, Boston, Massachusetts, USA, 2009), Vol. 1224, pp. 27.
[37] T. Aoyama, S. Yamazaki, and K. Imai, Japanese Journal of Applied Physics **39** (Part 1, No. 11), 6348 (2000).
[38] J. Assmann, V. Narkhede, N. A. Breuer, M. Muhler, A. P. Seitsonen, M. Knapp, D. Crihan, A. Farkas, G. Mellau, and H. Over, Journal of Physics: Condensed Matter **20** (18), 184017 (2008).